Colloquium: Experiments in vortex avalanches

E. Altshuler*

Superconductivity Laboratory and "Henri Poincaré" Group of Complex Systems, IMRE-Physics Faculty, University of Havana, 10400 Havana, Cuba

T. H. Johansen†

Department of Physics, University of Oslo, Blindern, N-0316 Oslo, Norway

(Published 29 April 2004)

Avalanche dynamics are found in many phenomena, from earthquakes to the evolution of species. They can also be found in vortex matter when a type-II superconductor is externally driven, for example, by an increasing magnetic field. Vortex avalanches associated with thermal instabilities can be an undesirable effect for applications, but "dynamically driven" avalanches emerging from the competition between intervortex interactions and quenched disorder may provide an interesting test scenario for nonequilibrium dynamics theory. In contrast to the equilibrium phases of vortex matter in type-II superconductors, the corresponding dynamical phases—in which avalanches can play a role—are only beginning to be studied. This article reviews relevant experiments performed in the last decade or so, emphasizing the ability of different experimental techniques to establish the nature and statistical properties of avalanche behavior.

CONTENTS

I. INTRODUCTION

Somewhere between physics and engineering, the critical-state model of Charles P. Bean (1962) continues to enjoy an immense popularity amongst those who need to understand the magnetic properties of almost all potentially useful superconductors. Above a certain magnetic-field threshold, type-II superconductors are penetrated by superconducting *vortices*, or flux lines, each one consisting of a normal-state core surrounded by a tiny supercurrent tornado with a few-dozen-nanometer radius. The vortices can therefore be thought of as long and thin solenoid magnets, which enter into the sample in increasing numbers as the external field grows. In a perfect superconducting crystal, the competition between the intervortex repulsion and the "magnetic pressure" from the outside field causes the vortices to arrange themselves in a hexagonal lattice (Abrikosov, 1957). In a real superconductor, however, there are defects acting as pinning centers, and the vortex motion becomes impeded. The interplay of pinning with an external drive "pushing in" more and more vortices results in a nonequilibrium state, the *critical state*, with a vortex density that is largest near the surfaces where flux enters the sample. This critical state typically involves several million vortices, and as the external field is increased or decreased, these readily organize themselves in spite of their short-range interactions. Researchers in the area of complexity would not hesitate these days to characterize Bean's critical state as an *emergent phenomenon* resulting from the *self-organization* of a *complex system* of vortices.

These are not empty words. They call attention to the fact that the collective, nonlinear statistical properties of a complex system can produce amazing macroscopic results, regardless of the details of the interaction between their microscopic constituents. They also suggest that we should look for analogies in other fields of science, even very distant ones. One such analogy is the comparison of Bean's critical state with a sandpile. As grains are added to a sandpile from the top, gravity tries to bring them off the pile, a motion prevented by intergrain friction. And again, in spite of the short-range character of the latter, the pile finds the way to organize itself and produce globally an *angle of repose*, or critical angle. In very simple terms, one can associate gravity with the magnetic field applied to superconductors, while friction corresponds to vortex pinning. This analogy might have appealed to Lord Kelvin, who once wrote "I am never content until I have constructed a mechanical model of the subject I am studying. If I succeed in making one, I understand; otherwise I do not" (Kelvin, 1884).

Grasping the similarities between a critical state and a sandpile well before the era of complexity as a subfield

*Electronic address: jea@infomed.sld.cu
†Electronic address: t.h.johansen@fys.uio.no

of physics, Pierre G. de Gennes comments in his classic 1966 book *Superconductivity of Metals and Alloys*: "We can get some physical feeling for this critical state by thinking of a sand hill. If the slope of the sand hill exceeds some critical value, the sand starts flowing downwards (avalanche). The analogy is, in fact, rather good since it has been shown (by careful experiments with pickup coils) that, when the system becomes overcritical, the lines do not move as single units, but rather in the form of avalanches including typically 50 lines or more" (de Gennes, 1966). This picture was not examined further for many years until scientists working in the field of complexity identified *avalanche dynamics* as a major mechanism in many physical, chemical, biological, and social phenomena. In particular, the idea of self-organized criticality (SOC) has found avalanches with "robust" power-law distributions of sizes and durations, underlying the dynamics of many systems (Bak, 1996; Jensen, 1998). With the sandpile as a central paradigm of SOC theory, Bean's critical state has become a natural place to look for avalanche dynamics. Although heroic efforts were made in the 1960s to see these avalanches, it was computer-controlled data acquisition that made it possible to investigate vortex avalanche *statistics* in superconductors. Other advances such as micro Hall probes and high-resolution magneto-optical imaging have finally given these studies contemporary validation. "Dynamically driven" avalanches like the ones suggested by the sandpile analogy can, after all, be the intrinsic mechanism in the formation of the critical state.

In Bean's time, another kind of vortex avalanche attracted most of the attention: the *flux jump*. Instead of helping to establish the critical state, flux jumps, which are thermally triggered, tend to destroy it. If the external field is increased too fast, and the thermal capacity and conductivity of the sample are small, the vortices rushing in will dissipate heat due to their motion, and the local temperature will rise. This tends to detach other vortices from their pinning sites, leading to new motion that can cause even further heating. This positive feedback process may sweep away the critical state in a large region of the sample and translate into a sudden, catastrophic decrease in magnetization. Thermally triggered avalanches have long been modeled in terms of macroscopic parameters. However, today's imaging techniques have provided data showing that these events sometimes also result in complex magnetic spatial structures which deserve a more detailed explanation.

All of these findings suggest that the simple analogy between sandpiles and vortex avalanches should be treated with caution: For one thing, temperature is not accounted for in the standard SOC picture. At this point, many questions arise: Can experiments reveal clear differences between dynamically and thermally driven avalanches? If so, can statistical analyses of the dynamically driven avalanches allow one to conclude whether Bean's critical-state model represents an SOC phenomenon? What is the relation between the magnetic flux distribution inside a sample and avalanche dynamics? Some experimental studies have attempted to address these subjects directly. Others offer relevant data as experimental "side effects." The available information can be characterized as scant, diverse, and entangled, and it is the purpose of this Colloquium to provide a coherent overview of the main results obtained in this area during the last decade or so.

II. THE NATURE OF VORTEX AVALANCHES

A. The critical state

When an external magnetic field exceeds the so-called lower critical field H_{c1}, the surface layer of a type-II superconductor begins to produce vortices, which immediately are pushed deeper into the material by the Meissner shielding currents. Each flux line consists of a "normal" core of radius ξ, the coherence length, surrounded by a circulating supercurrent decaying over a distance λ, the London penetration depth. The current is accompanied by an axial magnetic field decaying over the same λ, and integrates to a total amount of flux equal to the flux quantum $\Phi_0 = h/2e \approx 2\times 10^{-15}$ Tm^2, where h is Planck's constant and e is the elementary charge. As the applied field increases, the vortices get closer and closer until they overlap so much, that an overall transition to the normal state takes place at the upper critical field H_{c2}. When microscopic defects are present in the material, such areas tend to pin any vortex that passes by. The pinning force always acts against the driving force, which on a vortex has a Lorentz-like form, $\mathbf{f}_L = \mathbf{J}\times\Phi_0\hat{\mathbf{z}}$, where $\mathbf{J}$ is the local density of either a transport current or a magnetization current or both. The basic assumption of the critical-state model is that, as the vortices invade the sample, every pinning center that catches a vortex will hold onto it up to a certain maximum pinning force per unit vortex length, $f_p^{\max}$. In this way the local balance between the two competing forces, $|\mathbf{f}_L| = f_p^{\max}$, creates a metastable equilibrium state, where the current density adjusts itself to a maximum magnitude, $|\mathbf{J}^{\max}| \equiv J_c$, the Ampère critical current density. From Ampère's law it then follows that the flux density distribution $\mathbf{B}(\mathbf{r})$ in the critical state is given by

$$|\nabla\times\mathbf{B}(\mathbf{r})| = \mu_0 J_c . \tag{1}$$

The vortices therefore organize in such a way that their density decreases linearly from the edges of the sample, and the slope is $\mu_0 J_c$, as illustrated in Fig. 1(a). Shown in Fig. 1(b) is a set of B profiles that occur at different stages during an increase (left) and subsequent decrease (right) of the applied field. From the illustration it is evident that this strongly hysteretic process is quite analogous to what happens to a box of sand in which sand is added near the side walls (left), and then the walls are gradually lowered to zero height (right). The question is then: How do such systems evolve in space and time as they are driven externally through a continuous sequence of different critical states?

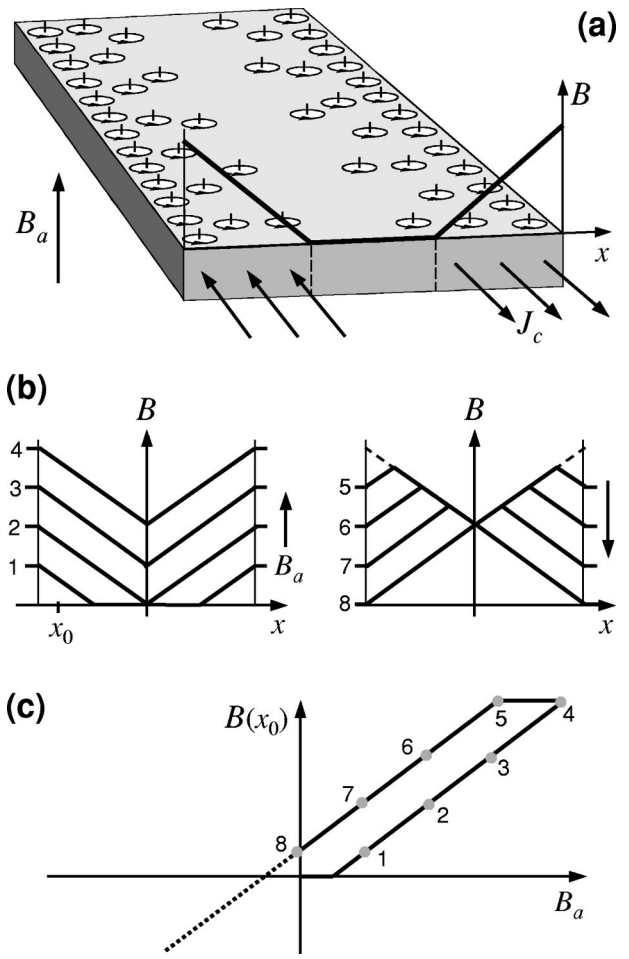

FIG. 1. Bean's critical state: (a) the distribution of vortices, internal field, and current in a superconductor placed in an external magnetic field B_a; (b) internal field profiles for increasing (left) and decreasing (right) B_a; and (c) variation of the local field at x_0 during the cycle in (b).

B. Dynamically and thermally driven avalanches

Dynamically driven avalanches in vortex matter are one possible way for the system to respond when subjected to a *slow* drive, e.g., a gentle ramping of the applied magnetic field. By driving the vortices sufficiently slowly one expects to control the dynamics via their mutual repulsion and interactions with pinning sites. If SOC provides the correct description, the critical-state behavior should show scale-invariant avalanche dynamics, i.e., a distribution of avalanche sizes that follows a power law, $P(s) \sim s^{-\alpha}$. Here $P(s)$ is the probability to find an avalanche event where s vortices suddenly move, and α is a critical exponent. While in the original formulation of SOC the exponent $\alpha \approx 1$ is found to be robust with respect to small changes in the model, later developments of the theory have shown that the exponent can vary within a certain range.

Note that in some cases temporal signals exhibiting scaling, e.g., signals with $1/f$ noise in the power spectrum, have been taken as direct evidence for SOC behavior. However, observation of $1/f$ noise should not be considered a sufficient indication of SOC, since it can result even from a spread of activation energies (O'Brien and Weissman, 1992; Jensen, 1998).

Whether real sandpiles follow the SOC scheme is still subject to debate (Held *et al.*, 1990; Bretz *et al.*, 1992; Rosendahl *et al.*, 1993, 1994; Frette *et al.*, 1996; Altshuler *et al.*, 1999), and a similar discussion extends to several other systems (Plourde *et al.*, 1993; Field *et al.*, 1996; D'Anna and Nori, 2000). It is therefore important to note that the critical state of type-II superconductors represents a unique and attractive case to study. In contrast to grains of sand, the vortices are noninertial objects and hence are closer to the idealized formulation of the SOC theory.

As in most areas where SOC ideas have been applied, the theoretical papers largely outnumber the experimental studies of vortex avalanches. Let us therefore, as a background for the main part of this Colloquium, mention briefly the important trends in the theoretical work, emphasizing ideas and results that most directly connect to the available experiments. Among computer simulation studies two philosophies dominate the literature; molecular dynamics and cellular automata. In addition, a few reports using a macroscopic approach have been published.

Most macroscopic treatments discuss vortex avalanches in a thermal activation scenario (Vinokur *et al.*, 1991; Tang, 1993; Pan and Doniach, 1994; Bonabeau and Lederer, 1995, 1996; Prozorov and Giller, 1999). Although some of these authors claim to find fingerprints of SOC behavior, their results are not compatible with the "canonical" formulation by Bak *et al.* (1987): As in a shaking sandpile, thermal activation causes the critical state to relax *away* from marginal stability because vortices, or bundles of them, jump out of their pinning centers and redistribute in such a way that the Bean's profile changes in time. This phenomenon, known as *flux creep*, was first observed by Kim *et al.* in 1963, and its typical manifestation is a slow, logarithmic temporal decay of the magnetization (Yeshurun, 1996). Thus flux creep can only be allowed within a "soft" definition of SOC; it will prove useful for interpreting certain relaxation experiments which will be discussed later in this Colloquium (Aegerter, 1998). There are also macroscopic studies that ignore flux creep effects. Barford (1997) proposes an equation of motion to analyze the dynamics of the critical state as the external field is increased and finds a power law in the distribution of avalanche sizes with a critical exponent of 1.13, consistent with the original SOC picture.

Molecular dynamics simulations typically allow integration of the equations of motion at the vortex level. Since this demands quite high computing power, the molecular dynamics work deals mostly with small systems. The cellular automata approach, on the other hand, simplifies the dynamics by selecting a set of physically sound rules that imitate the real laws, thereby allowing simulation of much bigger systems. Care must be taken, however, since the results can be sensitive to the selected set of rules (see, for example, Kadanoff *et al.*, 1989).

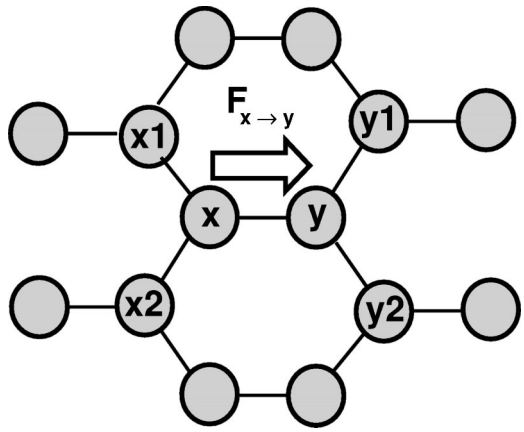

FIG. 2. Site lattice illustrating the Bassler-Paczuski cellular automata used for modeling vortex avalanches. Adapted from Bassler and Paczuski, 1998.

After the pioneering application of molecular dynamics techniques in the investigation of vortex avalanches in the critical state by Richardson *et al.* (1994), extensive work on the subject was generated (Barford *et al.*, 1993; Plá *et al.*, 1996; Olson, Reichhardt, Groth, Field, and Nori, 1997; Olson, Reichhardt, and Nori, 1997). A molecular dynamics simulation of a slowly driven critical state can be illustrated by the approach of Olson, Reichhardt, and Nori (1997): For every vortex, i, they solve the overdamped equation of motion

$$\mathbf{f}_i = \mathbf{f}_i^{vv} + \mathbf{f}_i^{vp} = \eta \mathbf{v}_i , \tag{2}$$

where $\mathbf{f}_i$ is the total force, comprised of the intervortex repulsion $\mathbf{f}_i^{vv}$ and the interaction between the vortex and a pinning center, $\mathbf{f}_i^{vp}$. The $\mathbf{v}_i$ is the vortex velocity, and η the "viscosity" of vortex flow. With this realistic description of each member of the ensemble, the simulations show that a critical-state flux profile builds up when vortices are slowly added from one side of the "sample." If one keeps adding vortices after the critical state is fully established, their effect can be followed by calculating the time evolution of the average vortex velocity. Typically, this shows bursts of activity, or avalanches, which resemble the voltage signals found in the pickup experiments discussed below (Field *et al.*, 1995). The avalanche size distribution resulting from these simulations follows a power law. When counting all the moving vortices for each avalanche event, one finds an exponent in the range $0.9 \leqslant \alpha \leqslant 1.4$, where the spread comes from varying the strength and density of the pinning sites. Similarly, for off-the-edge avalanches (counting only the number of vortices exiting through the "sample edge" during an event) one finds $2.4 \leqslant \alpha \leqslant 4.4$. Although these distributions are often well-behaved over quite a broad range, it is also clear that the exponent is not very robust.

The cellular automaton approach was introduced in a model by Bassler and Paczuski (1998), who considered vortex dynamics on a two-dimensional honeycomb lattice (see Fig. 2). Each cell x, which has three nearest neighbors, is occupied by an integer number of vortices. The authors then assume that the force pushing a vortex at x towards the neighbor cell y consists of two basic contributions: First, to mimic the vortex-vortex repulsion, the force increases as the population at x becomes bigger than that at y. A similar term representing the next-nearest-neighbor repulsion is also included. Second, to simulate the vortex-pin attraction, the force increases as the pinning potential at y becomes bigger than that at x (the pinning potential is represented by a random number assigned to each cell). In each time step, the cells are updated in parallel; a vortex moves to a neighboring cell if the force in that direction is positive. If a vortex is attracted in more than one direction, the selection can be made at random (Bassler and Paczuski, 1998) or by a largest-force rule (Bassler *et al.*, 2001). When vortices are now added at one edge of the "sample," this cellular automaton leads to a critical state very close to the ideal Bean's flux profile. As in the molecular dynamics simulations, this approach found avalanche dynamics, and the size distribution of the avalanches was reported to have a critical exponent of 1.63 ± 0.02 (obtained after finite size scaling for four orders of magnitude in avalanche size). In contrast to the molecular dynamics work, the exponent is here essentially constant within the range of parameters studied, therefore suggesting a SOC scenario (Bassler and Paczuski, 1998). The application of the model to the case of periodic, dense pinning indicates a slight decrease in the exponent to 1.45 ± 0.02 (Cruz *et al.*, 2000).

Besides SOC there are other theories producing power laws in the avalanche size distributions (Newman and Sneppen, 1996; Huang *et al.*, 1997; Carlson and Doyle, 1999; Schwarz and Fisher, 2001). Among these, the model of Newman and Sneppen (1996) seems the most relevant to the critical state, although the excitation in the form of "coherent noise" is not obviously applicable to vortex dynamics.

Catastrophic avalanches—flux jumps—are associated with a "runaway" in the motion of vortices as they redistribute in response to, say, an increasing applied field. Per unit volume, the motion generates heat at the rate of $J_c E$, where E is the electrical field. Due to this dissipation, the critical current density and thereby the shielding goes down, and more vortices rush into the sample. This positive feedback may or may not result in a flux jump. The superconductor is stable if the heat dissipation does not exceed the material's ability to store heat, a criterion that under adiabatic conditions can be expressed as (Mints and Rakhmanov, 1981)

$$\frac{\mu_0 J_c(T) w^2}{c} \left| \frac{dJ_c}{dT} \right| \equiv \beta < 1, \tag{3}$$

where c is the specific heat and w a typical dimension of the sample.[1] However, if $\beta > 1$, flux jumps are to be expected, and the first jump will occur when the field reaches the value $B_{\mathrm{fj}} \approx \sqrt{\mu_0 c (T_c - T)}$. Here T_c is the

[1] A prefactor of order unity is omitted in the formula.

critical temperature, and a linear $J_c(T)$ is assumed as a reasonable approximation. Let us put numbers on two cases that will be discussed later. For the 1.5×1.5-mm^2-area Nb foils used by Altshuler *et al.* (2002), one gets $\beta\approx5\times10^{-3}$, so flux jumps at the temperature of 4.6 K can be ruled out. For the mm-sized YBaCuO crystals studied in the sub-K range by Seidler *et al.* (1993) and Zieve *et al.* (1996), β becomes close to 3, and the situation is marginal. If flux jumps were to take place, they would here start at $B_{\rm fj}\approx5$ T, actually not very far from the threshold fields reported by these authors. However, estimates like these must be viewed with caution. No real experiment takes place under ideal adiabatic conditions, so other factors need to be considered as well. Generally, the "recipe" for avoiding flux jumps is to choose samples with high thermal conductivity, make sure that their thermal contact with the environment is good, and be gentle when ramping the applied field.

III. EXPERIMENTAL TECHNIQUES

The various magnetometric techniques used to measure vortex avalanches can be classified as either *global* or *local*. The global techniques are sensitive to either the amount of flux passing through the surface of the sample or the volume-averaged magnetic moment, whereas the local techniques detect the flux density or even the individual vortex positions in selected regions. In this section we give a brief overview of the various methods used in these experiments.

Pickup coil detection is the most basic global technique, and is typically configured as a coil wound tightly around the sample. When the external field is ramped up or down, the magnetic flux that enters or leaves the sample will (according to Faraday's law) induce a voltage in the coil proportional to the rate of this "traffic" of vortices. Therefore a steady-state flux motion results in a constant voltage output, while the appearance of spikes in the signal implies steplike increments, i.e., vortex avalanche events. By integrating the voltage over time one can determine, at least approximately, the amount of flux involved in such events, as was done in the careful experiments of Field *et al.* (1995), described in more detail below.

Another important technique is magnetometry using a superconducting quantum interference device (SQUID; see Barone and Paternó, 1982). The basic sensor here is a closed superconducting loop interrupted by, for instance, two Josephson junctions. A dc bias current is injected in such a way that it flows through the two junctions in parallel. If the loop is now subjected to a magnetic field, this produces a shift of the superconducting phase difference through the junctions, analogous to the phase difference between the various optical paths in Young's double-slit experiment. As a consequence, the maximum bias current that can be forced into the SQUID without dissipation becomes field dependent: $i_m(\Phi_{ext})=2I_{cj}|\cos(\pi\Phi_{ext}/\Phi_0)|$, where I_{cj} is the Josephson critical current of each junction and Φ_{ext} is the magnetic flux threading the SQUID loop. The periodic form of i_m implies that such a sensor can "intrinsically detect" magnetic flux with a resolution of less than one flux quantum. In practice, the field sensitivity of the SQUID depends on the loop area and on the design of the flux transformers. The areas of SQUID loops (or flux transformer pickup coils) typically extend from around 1 to 0.04 mm^2 (Lee *et al.*, 1995), the latter making it possible to apply the device for local measurements.

While sensors based on the Hall effect have long since proved very powerful, it was the invention of the modulation-doped semiconductor heterostructure (Dingle *et al.*, 1978) that gave rise to the present state-of-the-art sensors, the micro Hall probes. These epitaxial structures, mostly GaAl/AlGaAs, consist of 2D layers of electrons with large carrier mobilities at low temperatures. The active area of the sensing element ranges from 100 μm^2 to less than 1 μm^2. Note that, if just one flux quantum is present under a 100-μm^2 probe, the effective field is $\approx$0.2 Oe. Typically, this produces a Hall output of 2 μV for a bias current of 100 μA. Micro Hall probes today can also be manufactured as arrays of sensors in either linear or matrix arrangements. A practical linear array is composed of 11 square probes of 100 μm^2 each, separated by 20 μm center to center (Altshuler *et al.*, 2002). Micro Hall probes can also be attached to a piezoelectric scanner tube (as in a tunneling microscope) forming a scanning Hall-probe microscope (Bending, 1999). Such a device is able to scan the sample magnetically with submicron spatial resolution and resolve the field from individual vortices. A limitation of the method is that a standard scanning Hall-probe microscope can scan only small areas, typically 25×25 μm^2 at 77 K (Oral *et al.*, 1996).

The only technique that today allows experiments with combined high spatial and temporal resolution is magneto-optical imaging. Here the sensing element is a strongly Faraday rotating film, which one places directly on top of the sample under investigation. As illustrated in Fig. 3, the imaging is done by shining polarized light through the film, where reflection from a mirror, or the sample itself, gives the light a second pass that doubles the Faraday effect. The light then contains a distribution of rotation angles θ_F, corresponding to magnetic-field variations across the face of the superconductor. Finally, an analyzer set at 90° crossing relative to the polarizer filters the light and produces an optical image whose brightness shows directly how the magnetic field was distributed. Since magneto-optical imaging was invented in the 1950s several materials have been used as indicator films (Koblischka and Wijngaarden, 1995). During the last decade the most popular material by far has been the in-plane magnetization ferrite garnet films, often $(Lu,Bi)_3(Fe,Ga)_5O_{12}$, grown as a few-micron-thick epitaxial layer on gadolinium gallium garnet (transparent) substrates. The sensitivity of these indicators is represented by the low-field Verdet constant, $V=\theta_F/Hd$, where d is the film thickness. For green light (strongly present in Hg lamps) one has $V\simeq2°-8°$/kOe/micron, which is sufficient to resolve individual vortices (Goa

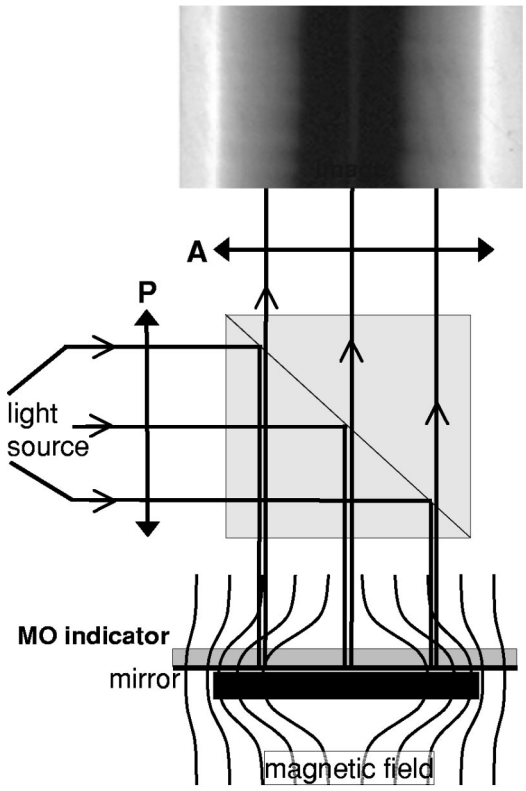

FIG. 3. Principle of the magneto-optical imaging technique. A magneto-optical (MO) indicator film placed on top of the superconductor gives the incoming polarized light a Faraday rotation according to the local magnetic field. After being reflected and passed through a crossed analyzer, the light produces an image in which the intensity contrast is a direct map of the field distribution.

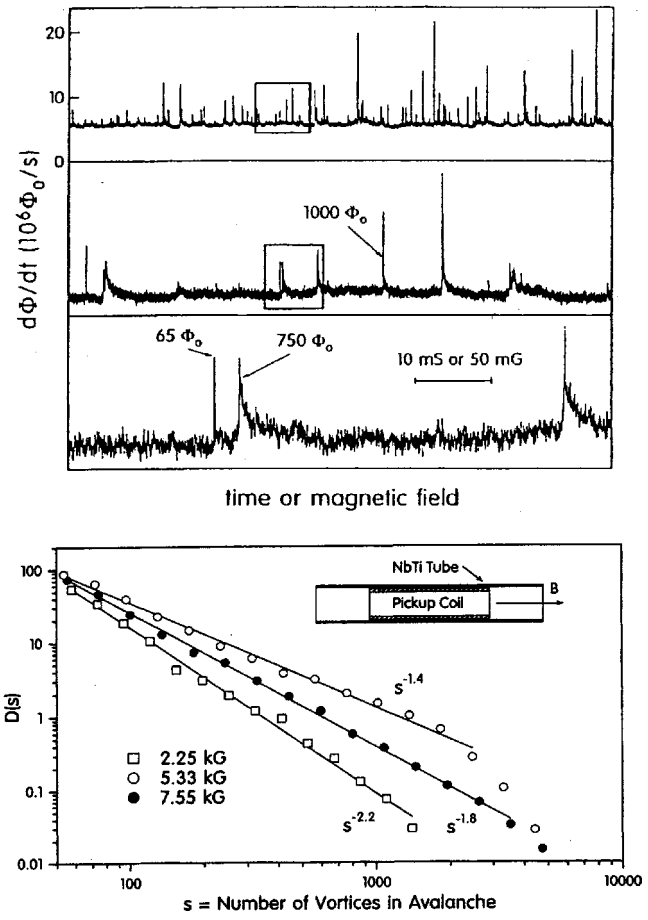

FIG. 4. Vortex avalanches reported by Field *et al.* (1995). Upper group of three panels: voltage output for different time windows, at a field window centered at 7.55 kOe. Note that the data shown in the small frames in the first and second panels are shown on an expanded scale in the second and third panels, respectively. Lower panel, avalanche size distributions for different field windows. The inset in this panel shows the experimental arrangement. Adapted from Field *et al.*, 1995.

et al., 2001). The unique power of the magneto-optical imaging technique is twofold; first, by simple optical means one may zoom between cm- and micron-sized fields of view, and second, the time response of the garnet film is extremely fast, of the order of nanoseconds (Runge *et al.*, 2000).

IV. REVIEW OF RECENT EXPERIMENTS

A. Pickup coil experiments

The first experiment on vortex avalanches inspired by the SOC ideas was reported by Field and co-workers in 1995 (Field *et al.*, 1995). An 1800-turn pickup coil was coaxially mounted on the inner surface of a tube made from the conventional superconductor NbTi. The tube had a 6 mm outer diameter, a wall thickness of 0.25 mm, and it was 3.4 cm long, nearly twice the length of the pickup coil. As noted by Field *et al.* (1995), this geometry guarantees a close analogy to (conical) sandpiles. An external magnetic field was applied along the tube axis at various ramp speeds, and the voltage induced in the pickup coil was amplified and recorded by a computer. The upper section of Fig. 4 displays the time variation of the signal over a field interval of 30 Oe centered at 7.55 kOe using the fairly low ramp rate[2] of 5 Oe/s. The authors identify two contributions to the flux penetration: The first, amounting to about 97% of the flux, corresponds to the background level and is believed to represent the thermally activated "smooth" flow of vortices. The second contribution is the set of well-defined spikes, which clearly indicate the presence of flux avalanches.

The lower panel of the figure shows the avalanche size distributions obtained from such experiments performed at three different fields. In each case the distribution follows a nice power law over more than one decade. The observed nonmonotonic change in the exponent from -1.4 to -2.2 is attributed by Field and co-workers to the different intervortex distances attained at the

[2]An accepted experimental meaning of a ramp rate being sufficiently low in the search for SOC behavior is that the resulting avalanche statistics become insensitive to the actual chosen rate. Typically, this occurs below 10 Oe/s.

various fields. This may be considered analogous to the influence of grain friction, shape (Frette *et al.*, 1996), and type of base (Altshuler *et al.*, 1999) on the similar exponents describing sandpile dynamics. The authors also report "1/*f*" noise in their experiments, finding power laws for low enough field ramp rates.

Let us take a closer look at how the avalanche size was determined in the work of Field *et al.* (1995). Consider a flux avalanche of length l—the length along the tube where a set of vortices "drops" out of the superconductor and spills into the hole where the coil is located. Only the corresponding number of turns, $n=lN/L$, where L and N are the coil's total length and number of turns, respectively, will pick up the flux change, and the coil responds by inducing the voltage $V=n\ (d\Phi/dt)$, where Φ/Φ_0 is the number of vortices participating in the event. From this the authors defined the avalanche size as an "effective bundle volume" given by $s\approx l\Phi=(L/N)\int V dt$. This is a convenient definition since it was not possible to determine l directly from the measurements.[3]

We suggest that the avalanche length l can be estimated using the collective pinning theory (Larkin and Ovchinnikov, 1973, 1979). According to it, the elastically deformed vortex lattice is characterized by the lengths L_c^b and R_c along, and normal to, the field direction, respectively (Blatter *et al.*, 1991, 1994). Over this volume the vortices are collectively pinned and behave essentially as one bundle. The value of l can be evaluated through the simple formula $l\approx L_c^b\approx(\lambda^2\xi^3/a_0^4)\times(J_0/J_c)^{3/2}$, where a_0 is the intervortex distance and J_0 is the depairing current density (λ, ξ, and J_c are defined in Sec. II.A). Substituting typical numbers for a low-T_c alloy at temperatures below 5 K (Campbell and Evetts, 1972), with a_0 corresponding to a few kOe field, we get an L_c^b of a few hundred microns (Altshuler, 2001), i.e., much smaller than the length of the pickup coil. Interestingly, a very early experiment by Wischmeyer *et al.* (1967), in which two separate coils—both similar to the one used by Field *et al.* (1995)—were mounted one after the other on the inside of a Nb tube, gave two more or less uncorrelated signals. The two coils were separated by a gap of 2.5 mm, supporting the above estimate for the size of the "avalanching objects."

In spite of the limitations inherent in the method used by Field *et al.* (1995), this paper was a catalyst for many studies of dynamically driven vortex avalanches in the second half of the 1990s.

B. Micro-Hall-probe experiments

In contrast to the pickup coil technique, Hall probes allow one to measure directly the size of the avalanching object in flux units. An avalanche event appears here as an abrupt step in the Hall signal, and the size of the step represents the change in the number of vortices populating the area under the probe. Such experiments were first carried out by Seidler *et al.* (1993), who with a Hall-probe area of $2\times10\ \mu m^2$ detected avalanches in 70-μm-thick, untwinned YBaCuO crystals during field ramps at 8 Oe/s. The measurements were made below 1 K, where they found relatively large events, and only above a certain field threshold. Although size distributions are not presented in this work, the observations suggest that in this case the avalanches were thermally driven, i.e., they were flux jumps.

Stoddart *et al.* (1993) performed similar experiments with slightly smaller Hall probes on 0.2-μm-thick films of Pb, and later also on Nb films (Stoddart *et al.*, 1995). Here, large avalanches were observed even in the beginning of the field sweep (ramp rate unknown), but again size distributions were not measured, thus preventing a comparison with SOC. However, from data obtained using a linear array of four micro Hall probes, the authors could determine the in-plane correlations of the avalanche behavior. This analysis identified an average flux bundle radius of $R_c\sim3.4\ \mu$m for Nb at $T=4.5$ K, in good agreement with the collective pinning theory.

Zieve *et al.* (1996) continued Hall-probe studies of avalanches in YBaCuO crystals, again performed at very low temperatures, even well below 1 K. Now the avalanche size statistics were reported, as well as hysteresis effects observed when the external field was cycled between 0 and 75 kOe. It was observed that the steps signaling avalanche behavior had a distinct onset field H_{up} during ascent, and that they disappeared on the descending branch at a much lower field. Since H_{up} is found to be essentially independent of the field ramp rate, Zieve *et al.* (1996) excluded the case in which the events are thermally driven. The avalanche size distributions turned out not to follow a power law, but instead to be sharply peaked around large-size (750 vortices) events, which is indicative of flux jumping and which is definitely not consistent with SOC. Nevertheless, Zieve *et al.* (1996) argued that their avalanches were dynamically driven and that a sandpile analogy would explain the observed hysteretic behavior: It is not equivalent to add grains to a pile (to increase the field) or to remove grains from its base (to decrease the field), because the overall weight of the pile is supported mainly by the grains at lower positions. To account for the peaked size distributions the authors extend the analogy. In their opinion, vortex mass renormalization (Blatter *et al.*, 1994) takes place at the very low temperatures of these experiments, making vortex inertial effects significant—and closer to some sandpile experiments, which show periodic avalanche events (Held *et al.*, 1990; Rosendahl *et al.*, 1993).

While SOC behavior was clearly *not* found in the experiments of Zieve *et al.*, it is not equally obvious that their explanation is fully germane: it is today believed that inertial effects are negligible even at these low temperatures (Vinokur, 2001). An alternative explanation is provided by Plá *et al.* (1996) and others (Olson, Reichhardt, Groth, Field, and Nori, 1997; Olson, Reichhardt,

[3]Detailed experiments by Heiden and Rochlin (1968) had already suggested similar limitations in the pickup coil setup.

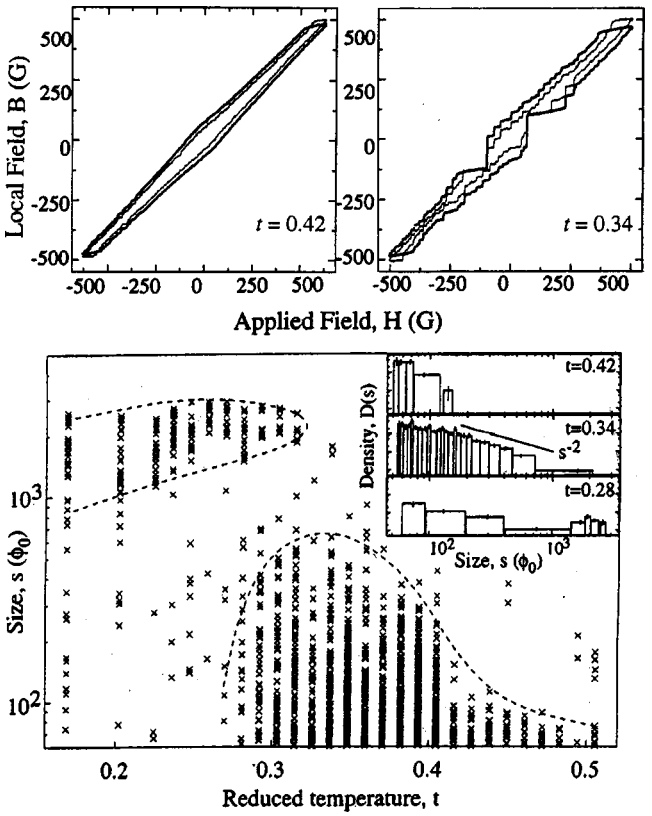

FIG. 5. Vortex avalanches reported by Nowak *et al.* (1997): Upper panels, local field vs applied field for two normalized temperatures, defined as $t=T/T_c$ [note the similarity with Fig. 1(c)]. Lower panel, avalanche size vs temperature diagram, and (inset) avalanche size distributions for different temperatures. Adapted from Nowak *et al.*, 1997.

and Nori, 1997), whose molecular dynamics simulations suggest that broad pinning centers with low density—as expected for the samples measured by Zieve *et al.* (1996)—produce peaked distributions of avalanches, while sharp and dense pinning—as expected for the samples measured by Field *et al.* (1995)—produces distributions closer to a power law.

Returning to low-T_c materials, Nowak *et al.* (1997) studied avalanches in Nb films of thickness $d=500$ nm. Their samples had an annular shape, with inner and outer diameters of 15 μm and 0.1 mm, respectively. Two 3×5-μm^2 Hall probes were used, one mounted over the central hole and one at a position 22 μm off center, allowing detection of the total flux involved in avalanches crossing the inner edge of the ring (center probe), and the local avalanche activity in the interior of the sample (off-center probe). Figure 5 contains the main results of Nowak *et al.* The upper two panels show how the local field varies as the applied field is cycled between ±500 G. The loops, obtained at different temperatures $t=T/T_c$, both contain distinct steps, and it is also evident that the magnitude and frequency of these avalanche events depend strongly on temperature. Moreover, by comparing the curves from the two probes (thick and thin lines represent the center and internal probe, respectively), one finds them not always correlated, showing that both global and local flux avalanches take place. The temperature dependence of this behavior is compiled in the lower part of the figure, where the main graph is a scatter plot of all the events detected by the center probe during two field cycles at each temperature. One sees that in a narrow range $0.3<t<0.4$ the distribution of avalanche sizes is broad and covers 1–2 decades. At lower temperatures $0.2<t<0.3$ the events cluster at large system-spanning sizes, typical for thermally triggered jumps,[4] and interestingly one finds at even lower t that the sizes again become broadly distributed. At $t>0.4$ only small avalanches occur, and the size distribution is monotonic and fits a decreasing exponential, as reported earlier by Heiden and Rochlin (1968). From the figure insets, one sees that a power law s^{-2} describes the distribution at $t=0.34$. In this work, the dependence of the avalanche activity on the ramp rate was also explored. In their range of rates, from 2 to 20 Oe/s, the behavior remained unaffected, showing that the system is in the slowly driven regime.

Nowak *et al.* (1997) explain these data on the basis of a thermally triggered mechanism. The analysis makes quantitative use of the stability parameter β, and both the superconducting film and the substrate are assumed to absorb heat. For the particular sample in this study one has unstable conditions from the lowest temperatures up to $t=0.37$, which is fully consistent with the numerous large-s events in this range and the rapid cutoff of large avalanches at higher t. The broad distribution of avalanches observed in the neighborhood of $t=0.37$ is related to β's becoming marginally greater than 1. Such a fine tuning of parameters may evidently give power-law behavior, at least over a size range of one decade or so. An alternative explanation for these findings is given by Olson, Reichhardt, and Nori (1997) based on molecular dynamics simulations. These authors suggest that, at low temperatures, pinning is so strong that interstitial motion of vortices takes place, resulting in peaked distributions of avalanche sizes. At higher temperatures the pinning decreases, so "pin-to-pin" vortex flow is allowed, giving rise to wide distributions of avalanche size closer to a power law.

While the ring configuration of Nowak *et al.* appears elegant, it should be emphasized that the critical state in thin films placed in a perpendicular applied field deviates quite dramatically from the picture shown in Fig. 1. In particular, for a ring-shaped superconductor, the central hole will contain a sizable nonuniform field due to shielding currents induced near the inner edge (Brandt, 1997). Actually, as the applied field is ramped from zero, there will be two flux fronts—one from each edge—advancing into the ring. The penetration from the inner edge consists of antivortices, because the edge field is here opposite to the applied field. As the field increases, the two fronts eventually meet [for the Nowak *et al.* (1997) geometry this occurs at ~3 μm from the inner

[4]This situation was also found in thin Nb films, although avalanche size statistics were not reported (Esquinazi *et al.*, 1999).

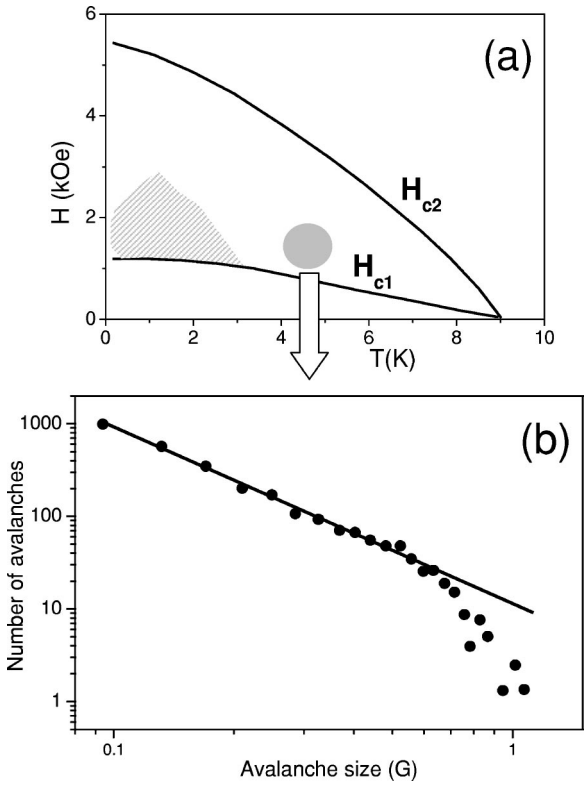

FIG. 6. Vortex avalanches reported by Behnia *et al.* (2000): (a) Catastrophic avalanches take place in the dashed area of the H-T diagram, while small ones occur in the rest of the region between the two lines; (b) typical avalanche size distribution corresponding to the small-avalanche region indicated by the gray circle in the H-T diagram. Adapted from Behnia *et al.*, 2000.

edge] and annihilation of the two vortex species takes place. We find that the actual field when this occurs is $H_c \simeq J_c d \simeq 150$ G, if we assume a value of $J_c = 2 \times 10^6$ A/cm^2 for the Nb film. It is clear that the sample of Nowak *et al.* (1997) was cycled through a set of magnetized states with quite complicated flux distributions, where purely geometrical (or demagnetization) effects may preclude direct analogies to sandpile dynamics.

The first spatio-temporal study of internal vortex avalanches was made by Behnia *et al.* (2000), who made their measurements on a 20-μm-thick foil of Nb cut as a square with sides of length 0.8 mm. Unlike previous studies, this work explored the whole H-T region between H_{c1} and H_{c2} [see Fig. 6(a)]. At low temperatures, indicated by the hatched area, Behnia *et al.* found catastrophic, flux-jump-like avalanches. Outside this region the behavior was qualitatively different, as exemplified by the results of the following experiment made at 4.8 K with an applied field around 1.5 kOe (start of the vertical arrow in the phase diagram).

A 0.35-mm-long Hall-probe array consisting of eight equally spaced 20×5-μm^2 probes, each one with a sensitivity of $0.16\Phi_0$, was mounted on the sample along a line normal to one of the sides. After checking that the field created a Bean-model flux density profile—something that was difficult to assess in previous experiments due to the small numbers of Hall sensors—Behnia and co-workers made a series of measurements as the field was increased from 1.5 kOe at the rate of 1.1 Oe/s. From each probe, they found a local field varying in steps, much like those reported by Nowak *et al.* (1997). The avalanche size statistics obtained by analyzing the signal from one probe is shown in Fig. 6(b). In the small-event region the size distribution follows a power law with an exponent of -2.1 (fitted line), which is within the range of exponent values reported by Field *et al.* (1995). Deviations from the straight line start around 0.6 G and reflect a clear deficiency of large events. Note that the largest avalanche event is a field step of 1.1 G, corresponding to a sudden entry of five vortices into a probe area already populated by more than 6000 vortices. The authors leave the lack of large avalanches an open question. Could failure to wait for the extremely rare events be the simple explanation?

Behnia and co-workers also investigated the temporal correlations of avalanches by comparing the signal from Hall probes located at 50-μm distance from each other. They estimated an average transit time of 0.8 ms, which gives an avalanche speed of a few cm/s. This can be compared with the velocity of vortex motion during flux flow, given by $v \sim \rho_n J_c / \mu_0 H_{c2}$, where ρ_n is the normal-state resistivity. This gives velocities in the range of 25–8000 cm/s for parameters near the measuring conditions of Behnia *et al.* (2000). Since thermal activation and a possible current dependence of the resistivity would decrease this estimate, we conclude that the velocities of these avalanches, which have a broad size distribution, are consistent with a simple picture of vortex motion, in strong contrast to the ultrafast dendritic flux penetration discussed later (in Sec. IV.C).

Pushing the Hall-probe technique even further, James *et al.* (2000) used a high-resolution scanning Hall-probe microscope to look at flux penetration into a 1-μm-thick Nb film shaped as a 100-μm-wide strip. As the applied field was slowly swept up and then down, they found (by keeping the sensor stationary 25 μm from the edge) a steplike behavior in the Hall signal, much as in previous observations. But new aspects of the behavior were uncovered when the probe was scanned across a large part of the sample area. This showed that the flux does not penetrate with a smooth advancing front, but instead as a series of irregularly shaped protrusions. These protrusions were easily distinguished from the much larger and blob-shaped flux patterns that sometimes form abruptly during field sweeps at temperatures below 4 K. Whereas the blobs are firmly believed to be the visible result of conventional flux jumps, James *et al.* (2000) speculate about the origin of the numerous protrusions, which are apparent at all temperatures up to T_c. A key observation is that when the protrusions invade the flux-free Meissner region the neighboring "fingers" show a strong tendency to avoid each other. Had the protrusions been the fingerprint of scratches or other defects facilitating easy flux penetration in the film, this kind of behavior would be very unlikely. Instead, James *et al.* suggest that some long-range repulsive force plays a role here, and

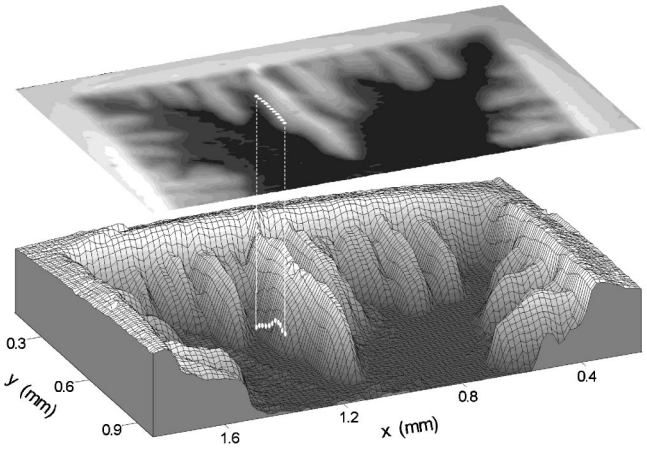

FIG. 7. Magnetic landscape in a Nb foil where an array of micro Hall probes (white dots) detect avalanches coming down the slope of the largest "flux ridge" (Altshuler *et al.*, 2002). In the bottom graph, the intensity along the vertical axis is proportional to the magnetic field inside the sample. From Altshuler *et al.*, 2002.

indeed such an interaction does exist between vortices in thin samples. In contrast to the exponential dependence in bulk, for thin superconductors in a perpendicular field there is a long-range inverse distance-squared decay of the vortex-vortex force due to their surface screening currents (Pearl, 1964). Therefore it may well be that flux penetration in the form of these protrusions is an example of a dynamically driven vortex system full of avalanche dynamics. The differences between penetration patterns at two fields differing by 10 G revealed that the flux front advances by an apparently random sequence of localized bursts of flux motion. The size of these events was found to vary, but James *et al.* (2000) do not report quantitative size statistics of any kind.

So far, all the mentioned studies of vortex avalanches and their statistics, i.e., those in which SOC ideas were examined using micro Hall probes, have lacked information about the actual "magnetic landscape" in which the probes were located. Furthermore, the number of recorded avalanches have been fairly limited, estimated to be around 150 events in the experiments of Zieve *et al.* (1996) and 5000 events in those of Behnia *et al.* (2000), and thus hardly sufficient to convincingly establish power laws when broad size distributions are found. Both these shortcomings were largely improved by Altshuler and co-workers (Altshuler *et al.*, 2002) who combined magneto-optical imaging with the recording of many long series of Hall-probe data. Also the sample used was a Nb foil, 30 μm thick and cut into a square with 1.5-mm sides. Figure 7 shows a magneto-optical image of flux penetration into the sample and reveals that the distribution does not correspond to a simple sample-spanning critical state, but rather to a set of flux ridges, each having an "inverted V," Beans-like profile. In this landscape an 11-probe Hall array, with 10×10-μm^2 sensor areas, was mounted on the slope of the largest ridge,

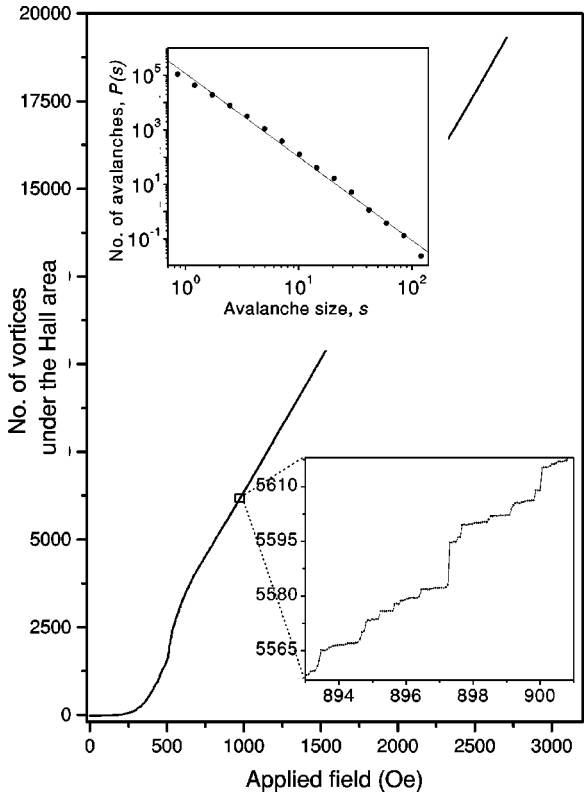

FIG. 8. Vortex avalanches reported by Altshuler *et al.* (2002): main curve and lower inset, evolution of the number of vortices under the Hall-probe areas seen in Fig. 7 as the external field is increased; upper panel, resulting avalanche size distribution. From Altshuler *et al.*, 2002.

as indicated by the set of white dots[5] in Fig. 7.

Shown in Fig. 8 is the signal from one of the Hall sensors recorded as the field was ramped from 0 to 3.5 kOe at 1 Oe/s and $T=4.8$ K. When the curve is examined in detail (see lower inset), one finds clear signatures of avalanche dynamics over the whole range of fields. The data from all of the 11 probes for repeated numbers of experiments made under the same conditions, were registered and analyzed, amounting to several hundred thousand events. The resulting size distribution is plotted in the upper inset of the figure, which shows that the avalanche sizes covering two decades follow a power law with a slope of -3.0 ± 0.2. To check the robustness of this result, the authors explored the avalanche behavior at many locations by remounting the Hall array at various positions in the landscape. A power-law behavior was found everywhere, and the exponent was essentially the same. The observed robustness gives grounds for the claim to have, for the first time, observed SOC in flux dynamics.

[5]Magneto-optical imaging experiments were recently made by the authors (specifically for this Colloquium) on Nb foils kindly provided by K. Behnia. It was found that for samples similar to those studied by Behnia *et al.* (2000) the flux penetration is globally non-Bean-like and quite similar to that one seen in Fig. 7, at least below 500 Oe.

In an attempt to investigate the rigidity of the vortices involved in these avalanches, a pair of Hall arrays were mounted on the two sides of the Nb foil with the probes directly facing each other (Altshuler *et al.*, 2002). The analysis of cross correlations in these data indeed shows *some* degree of correlated behavior on the two sides of the sample, which is most clearly visible for the larger avalanches.

Very recently, Radovan and Zieve (2003) used a micro Hall probe of 400 μm^2 area to look at the avalanche behavior in type-II, Pb thin films of 100 nm thickness. The external field was slowly ramped up to 400 Oe, at various temperatures between 0.27 and 5.9 K. The authors found large avalanches at relatively high temperatures and "micro-avalanches" at lower temperatures. Based on these observations they report power-law distributions of avalanche sizes at the two temperatures 0.3 and 4.3 K, with exponents of 2.0 and 1.1, respectively.

Three other recent papers report avalanches observed by micro Hall probes, although without including avalanche size statistics. Shung *et al.* (1998) found noncatastrophic vortex avalanches on a single-crystal torus made from the heavy-fermion superconductor UPt_3. The authors suggest that the observed sharp temperature onset for the appearance of avalanches is an indication of broken time-reversal symmetry. Ooi *et al.* (2000) found signs of SOC in the $1/f$ noise spectrum they obtained from the analysis of avalanches found in $Bi_2Sr_2CaCu_2O_8$ single crystals.[6] The same kind of sample was also studied by Milner (2001), who found huge avalanches in the region below 1 K and up to 17 T that strongly resemble those reported by Zieve *et al.* for YBCO crystals. Milner proposes a number of possible explanations for the phenomenon, ranging from domain structures that modulate the interplay between interpin and intervortex spacings, to broken time-reversal symmetry in his samples.

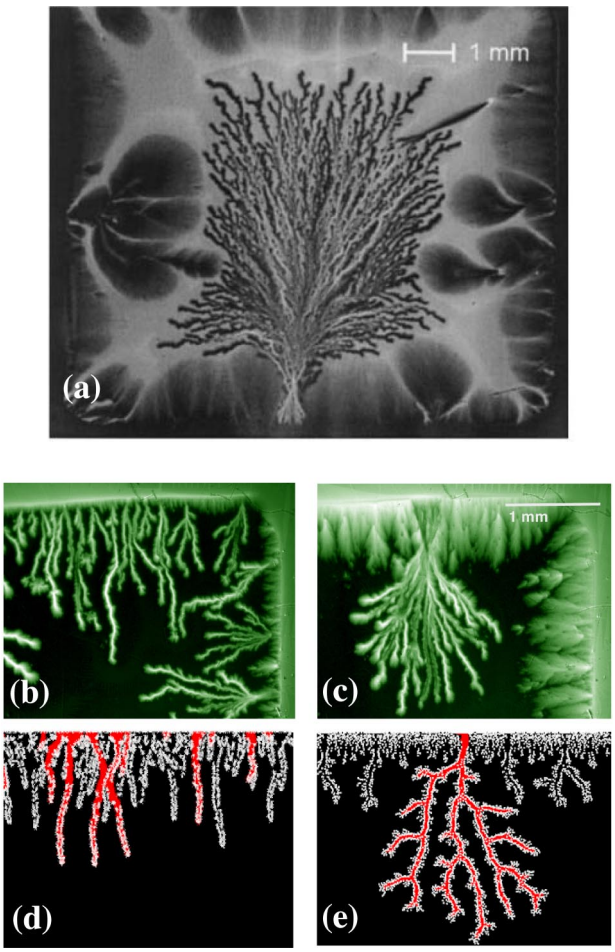

FIG. 9. (Color in online edition) Flux dendrites formed abruptly in thin-film superconductors: (a) In YBaCuO at $T = 4.2$ K; (b) and (c) In MgB_2 at $T = 3.8$ and 10 K, respectively; (d) and (e) by vortex dynamics simulations made for low and high temperature (see text). Panel (a) is from Leiderer *et al.*, 1993 and panel (b) from Johansen *et al.*, 2002.

C. Magneto-optical imaging experiments

The use of the space- and time-resolving power of magneto-optical imaging to study flux motion was pioneered in the 1960s. Inspired by the visualization work of DeSorbo and Newhouse (1962), Wertheimer and Gilchrist (1967) used a fast camera technique to study how flux penetrates into disks of Nb, V, and various alloy superconductors. As the applied field was increased, they found events of abrupt flux invasion starting from a point along the perimeter. One particular observation was crucial in understanding the nature of these avalanches, namely, that the events were accompanied by bubbles formed in the liquid coolant right above the sample surface. It was evident that thermomagnetic flux jumps had, for the first time, been directly observed. These early experiments also showed that the bursts of flux motion fell into two categories: "smooth" and "irregular" (or branching), referring to the geometrical shape of the invading flux front. The two types of avalanches were found by Wertheimer and Gilchrist (1967) to be related to sample quality: smooth jumps were typical for "pure" samples, while the branching patterns were seen only in the alloy disks, suggesting that material inhomogeneities drastically perturb the course of the avalanches.

Then, in 1993, the branching scenario of flux penetration was revisited by Leiderer *et al.* (1993) making full use of the high spatial and temporal resolution offered by the ferrite garnet indicator films. A typical pattern, this time observed in thin films of YBaCuO, is shown in Fig. 9(a). These magnificent dendritic patterns were triggered by perturbing a flux-filled remnant state with a laser pulse fired at a point near the sample edge. This heated spot became the root of the branching structure, which is where the trapped flux escaped the sample. The study revealed that if the experiments were repeated in exact detail, the branching forms would nevertheless vary widely. In other words, these events produce "ir-

[6]These experiments cannot be easily compared to others presented in this Colloquium, since they do not involve a slow increase of the applied field at a fixed temperature.

regular" flux patterns that are *not* controlled by quenched disorder in the sample.

Soon after, Durán *et al.* (1995) found essentially the same spectacular behavior in films of Nb. This time the dendritic flux patterns were produced by simply lowering the field from 135 Oe applied during the sample's initial cooling to various temperatures below T_c. These films were 500 nm thick, and the overall conditions closely resembled the descending field branch in the Hall-probe experiments of Nowak *et al.* What the magneto-optic imaging revealed was that the dendritic patterns actually vary in their morphology, changing from quasi-1D structures at temperatures below $0.35T_c$, to highly branched structures *à la* the one seen in Fig. 9(a) at temperatures approaching $0.65T_c$. These findings strongly suggest that the cluster of large events at the lowest temperatures reported by Nowak *et al.* (1997) are due to the abrupt formation of such macroscopic dendritic structures (Jaeger, 2000).

Dendritic avalanches with the same qualitative characteristics were observed quite recently also in films of MgB_2 (Johansen *et al.*, 2001, 2002), and Nb_3Sn (Rudnev *et al.*, 2003), only here, as in the very early magneto-optical imaging experiments, the abrupt events were triggered simply by ramping up the applied field. During slow ramps after zero-field cooling to 4 K, the films became invaded by numerous dendrites, which burst into the Meissner state region one at a time for the case of MgB_2 [see Fig. 9(b)]. Near 10 K, the dendritic structures became much larger, as in (c), whereas at even higher temperatures and up to $T_c = 39$ K such "irregular" features ceased to be formed. What is the nature of this type of avalanches, and why do they take the form of branching flux dendrites? To find the answer, one should note from Fig. 9 that the dendrite fingers have a strong tendency to avoid overlapping. As discussed in relation to the work of James *et al.* (2000), this is probably a result of the long-range action of the repulsive force between vortices in thin films. The same "explosive" force could also be responsible for the branching itself, although the mechanism for selecting these seemingly random bifurcation points is not yet clear.

These observations formed the basis for a molecular dynamics computer code (Johansen *et al.*, 2002), in which the dynamical equation (2) was modified to account for the thin-film geometry by using $1/r^2$ intervortex forces and adding a term for the Lorentz force from the Meissner currents, which in thin superconductors flow over the whole area. Finally, a thermal component was introduced: When any vortex i moves a distance Δr_i, given by evaluating v_i, an amount of heat, $Q_i = \Delta r_i f_i$, is produced that raises the temperature in the neighborhood of the trajectory by $\Delta T \propto Q_i$. This then has a direct effect on the local pinning conditions, since the pinning force is taken to be T dependent (as $f_i^{vp} \propto 1 - T/T_c$). The results of these simulations can be seen in Figs. 9(d) and (e), showing flux penetration patterns corresponding to low and high temperatures, respectively. Notice that some of the dendritic fingers have a "spine," which is an instantaneous map of the temperature rise due to recent traffic of vortices penetrating from the upper edge. Clearly, the avalanche morphology found experimentally is very well reproduced by these simulations. Analytical efforts have addressed the same question. Calculations by Aranson *et al.* (2001) suggest that vortex "micro-avalanches" can be triggered by a hot spot and that the temperature distribution can evolve in a branching manner. Despite the qualitative success of the theoretical work, more needs to be done to understand these avalanches at a quantitative level. For example, magneto-optical imaging using double-pulse laser illumination with time intervals less than 10 ns has shown that the speed of dendrite propagation in YBaCuO is close to 25 km/s (Bolz, 2002). This is orders of magnitude higher than the avalanche velocity reported by Behnia *et al.* (2000), and actually the two scenarios appear totally different, as one would expect for dynamically and thermally driven systems. Interestingly, the speed of dendrite propagation even exceeds the velocity of sound in the material, raising questions about which nonphonon heat conduction mechanism is at work here.

Very recently, magneto-optical imaging was used to study noncatastrophic avalanches. In the work of Bobyl *et al.* (2003) the first spatially resolved observation of vortex avalanches on a mesoscopic scale is reported. A thin film of MgB_2 was investigated at temperatures below 10 K, where flux dendrites can form in this material, but the applied field was now kept below the threshold for dendrite formation. By increasing the field slowly (60 mOe/s) Bobyl *et al.* were able to observe avalanches by subtracting subsequent images recorded at intervals of $\Delta H = 0.1$ Oe. All the avalanches had a regular shape with no sign of ramification, and they appeared at seemingly random places, mainly near the edge of the film. The total number of vortices participating in an avalanche varied between 50 and 10 000. However, the work does not report any detailed statistics. Interestingly, the mesoscopic avalanches, having a typical linear size of 10–20 μm, continued to form at higher fields, where large dendrites dominated the flux penetration. Moreover, it was found that, above 10 K, both types of avalanches (mesoscopic and dendritic) ceased to form, suggesting that only one physical mechanism was responsible for both.

Aegerter *et al.* (2003) subjected an 80-nm-thick film of YBaCuO, after zero-field cooling to 4.2 K, to a perpendicular field slowly increased in a stepwise manner. After each field step of 0.5 Oe, the sample was allowed to relax for 10 s before an image was taken. By subtracting subsequent images, Aegerter *et al.* obtained the difference in flux density $\Delta B_z(x,y)$ and integrated over a subarea, $L \times L$, of the total field of view. This revealed clearly that the evolution of the magnetic flux inside the sample was intermittent, with occasional bursts of various sizes. To allow for a finite-size scaling analysis, the authors let L vary between 180 and 15 μm (see Fig. 10). The histogram of avalanche size distributions with four different L values shows power laws, which when combined extend over more than three decades. Further-

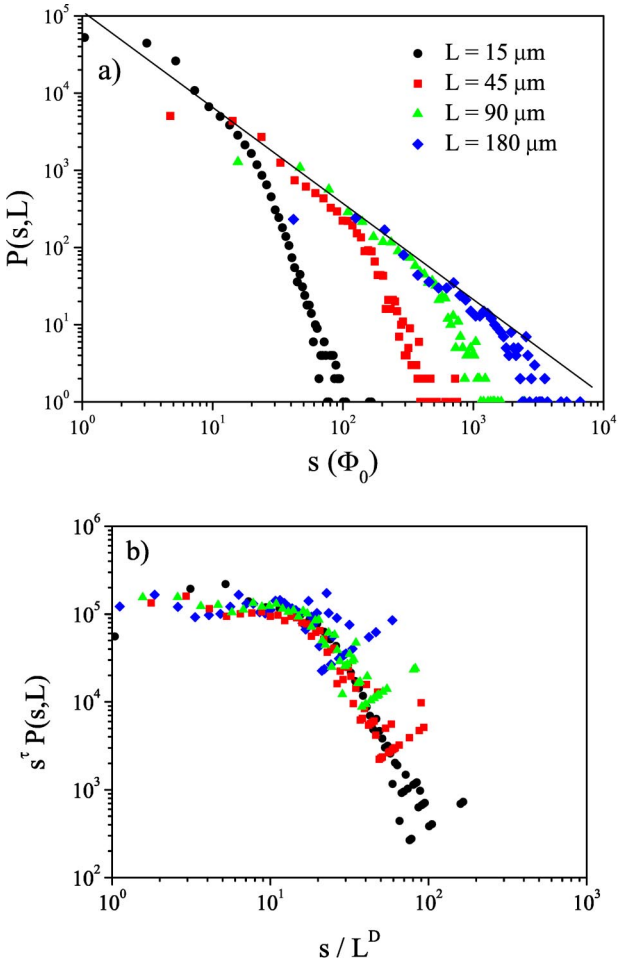

FIG. 10. (Color in online edition) Avalanche size distribution obtained from magneto-optical imaging of flux penetration in a YBaCuO film: (a) the direct avalanche distribution using observation windows of different size $L \times L$; (b) scaled plot of the four curves in (a) showing that they possess finite-size scaling. From Aegerter *et al.*, 2003.

more, plotting the histogram versus the scaled avalanche size, s/L^D, shows that the data are well fit using $\alpha = 1.29$ and $D = 1.89$. In addition, the authors measured both the so-called roughness exponent and the fractal dimension of the avalanche clusters, and showed that the set of exponents obeyed a universal scaling relation. This is a strong indication that SOC is present in their system.

Related to this is the earlier observation of kinetic "roughening" of advancing flux fronts in high-T_c films (Surdeanu *et al.*, 1999). By applying scaling analysis, these authors showed that there are two regimes: at small length scales or short time scales, where static disorder dominates and where the roughening and growth exponents correspond to a directed-percolation-depinning model. In contrast, at larger scales, temporal stochastic noise dominates and the exponents come close to those of the Kardar-Parisi-Zhang (1986) model. This finding has common ground with findings of the dynamically driven avalanche community: theoretical models of sandpiles have established relations between

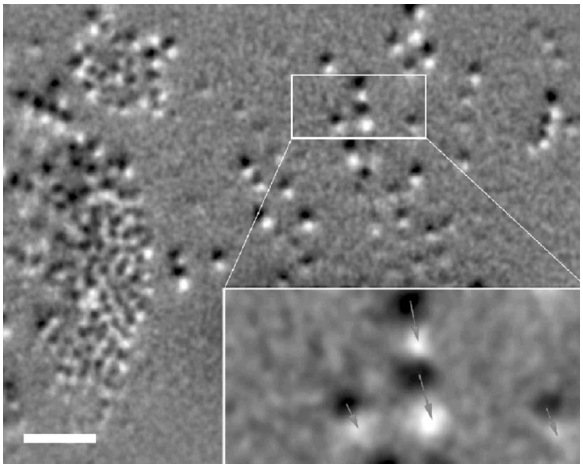

FIG. 11. Vortex avalanches in $NbSe_2$ observed by magneto-optical imaging. The bright and dark dots show where vortices have moved to and from, respectively, during a field step of 4 mOe. The scale bar is 10 μm long.

the critical exponents of avalanche dynamics and those for interface growth, including for the Kardar-Parisi-Zhang model (Paczuski and Bassler, 2000; Chen and Nijs, 2002).

The magneto-optical imaging technique made a giant leap forward when Goa *et al.* (2002) succeeded in resolving individual vortices, thereby directly observing their motion. This work introduced a new method capable of following vortex avalanche dynamics in full detail,[7] and not only through sampling of the flux density integrated over some area. In particular, single-vortex-resolution magneto-optical imaging offers a way to study experimentally the role of interstitial versus "pin-to-pin" motion of vortices during avalanches, as predicted in molecular dynamics simulations (Olson, Reichhardt, Groth, Field, and Nori, 1997; Olson, Reichhardt, and Nori, 1997). It could also shed light on the details of "braided rivers" of vortices resulting from cellular automaton simulations (Bassler *et al.*, 1999). To illustrate what is now possible, Fig. 11 shows the difference of two magneto-optical images recorded before and after the applied field was increased on a superconducting 0.1-mm-thick single crystal of $NbSe_2$ at 4 K. The bright and dark dots show the local increase and decrease of the field, i.e., they are the positions the vortices have hopped to and from, respectively. The areas where such dots are absent also contain vortices, but they have not moved during this particular interval. From the image one can clearly identify vortex avalanches of various sizes. For example, there is a quite large event taking place on the left side, and many small ones, down to individual hops, are scattered over the whole field of view. Although this new high-resolution magneto-optical imaging method

[7]Compared to Lorentz microscopy, the only other method with the same capability, magneto-optical imaging is not restricted to samples so thin that the electron beam goes through.

TABLE I. List of experiments reporting vortex avalanche size distributions. The information in the table was extracted directly or indirectly from the references cited. Distributions are abbreviated as follows: Exp, exponential; peak, peaked; power (exponent), power-law; stexp, stretched exponential.

Reference	Geom.	Material	Sensor	Avalanche type	T/T_c	H range (kOe)	Rate (Oe/s)	Avalanche distribution
Heiden *et al.* (1968)	hollow cylinder	Pb-In	pickup coil	off-edge	0.6	0.55–0.85	10–100	exp
Field *et al.* (1995)	hollow cylinder	Nb-Ti	pickup coil	off-edge	0.3	2.25–7.55	5	power (1.4–2.2) (slow ramps)
Zieve *et al.* (1996)	planar	YBCuO crystal	Hall probe	internal	$\leqslant 0.01$	0–80	7	peak
Nowak *et al.* (1997)	planar ring	Nb film	Hall probes	off-edge & internal	0.15–1.12	-0.5–0.5	0.002–20	peak/power (2.0)
Aegerter (1998)	planar	BSCCO crystal	SQUID	off-edge	0.06–0.8	?	0	exp/power (2)
Behnia *et al.* (2000)	planar	Nb film	Hall probes	internal	0.52	1.5	~ 1	peak/power (2.05) /stexp
Altshuler *et al.* (2002)	planar	Nb foil	Hall probes & MOI	internal	0.5	0–3.5	~ 1	power (3.0)
Aegerter *et al.* (2003)	planar	YBCO film	MOI	internal	0.05	0–0.15	$\leqslant 0.05$	power (1.30)
Radovan and Zieve (2003)	planar	Pb film	Hall probes	internal	$\leqslant 0.7$	0–0.04	0.2–3.3	peak/ power (1.1,2.0)

has not yet been used specifically to study avalanches, it is evident that its experimental potential is huge and will bring us closer to a full understanding of vortex dynamics.

D. Miscellaneous experiments

Vortex avalanches not associated with conventional flux jumps have also been detected through other techniques like SQUID magnetometry (Wang and Shi, 1993; Aegerter, 1998; Kopelevich and Moehlecke, 1999) and torque magnetometry (Hope *et al.*, 1999). Among these observations, only those of Aegerter (1998) reported avalanche size distributions obtained by studying the detailed flux motion during creep in a $Bi_2Sr_2CaCu_2O_8$ crystal. Instead of driving the vortices by increasing the applied magnetic field, Aegerter *et al.* created the avalanches by thermal activation in a constant applied field. Using a SQUID sensor they recorded the events over a period of more than 10^5 s. The main finding was that at low temperatures ($0.06T_c$) the distribution of avalanche sizes showed power-law behavior, whereas at higher temperatures ($0.8T_c$) the distribution became exponential. A theoretical discussion of these results has been provided by Mulet *et al.* (2001), based on the Bassler-Paczuski (1998) cellular automaton with additional Monte Carlo rules to account for the slow thermal activation. They conclude that the critical exponents obtained in creep experiments can be related to, but are not identical to, those predicted in the original SOC scheme.

Table I summarizes the main results concerning avalanches, along with the experimental conditions reported in all the papers reviewed in this Colloquium.

V. SUMMARY AND OPEN QUESTIONS

When an account of a given scientific subfield is written long after the key developments, a filtering process takes place which results in a nice *concerto* of experiments, perfectly aimed at the "big question." However, in the case of vortex avalanche experiments immediacy has forced us to replace such an ideal approach by a more disjointed report on recent progress. Nevertheless, we have still been able to distill from the available experiments a set of issues and questions that may contribute significantly to an understanding of the physics behind vortex avalanches.

Although low-T_c materials dominate most of the experiments in which avalanche size statistics are reported, the types of samples used vary widely (cylinders, films, foils) and the temperatures, field ranges, and field sweep rates also vary quite a bit from experiment to experiment. The occurrence of avalanches in the different regions of the H-T phase diagram has been only rarely explored. In practice, it has proved difficult to tell if the observed avalanches are thermally or dynamically triggered, although there is consensus that thermally driven avalanches abound at T below 4 K or so—at least in low-T_c samples. Remarkably, only one piece of experimental work on high-T_c materials reports finding noncatastrophic avalanches while a field is slowly increasing. Is this general situation due to a lack of instrumental resolution, or perhaps are the avalanches just "smoothed out" by thermal activation?

Even when noncatastrophic avalanches are detected as the field is swept, opinions are divided as to their origin. Some authors claim that self-organized criticality is at the core of the dynamics. But robust, well-defined power laws have proven somewhat elusive: Nature does

not seem to like more than two decades of avalanche sizes measured in a single experiment . . . or have we failed to be patient enough to collect the appropriate wealth of data (Avnir *et al.*, 1998)?

Some simulations suggest that the type of avalanche size distribution may depend on the nature and density of pinning sites—in analogy with experiments in sandpiles with different types of grains and bases on which the piles are grown. Definitive experiments to check this hypothesis can be performed only on samples with artificially tailored pinning landscapes. If this suggestion is true, could measurements of avalanche size distributions become a tool to figure out the pinning features of a given sample?

In the case of noncatastrophic events, and when power-law behavior is found, there is a great dispersion in the critical exponent of the avalanche size distributions. This applies to both experiment and theory. While for the first category the exponent ranges from 1.3 to 3.0, in the second it typically extends from 1 to 2, and it can go even further. An important question in principle then arises: Is it possible to establish a one-to-one correspondence between the different experiments and models?

Power-law distributions of avalanche sizes are expected to be associated with linear flux profiles (as originally proposed by Bean), since nonlinear ones, in principle, cannot result in scale-invariant avalanches. Many of the recent experiments have been made on thin superconductors in a perpendicular magnetic field where the flux density profiles have an enhanced slope near the sample's edge and center. This applies even for samples with a constant critical current density (Zeldov *et al.*, 1984). In bulk samples there is also the possibility of nonlinear profiles due to a B dependence of the critical current density, e.g., as in the Kim model (Kim *et al.*, 1963). What exactly are the differences in avalanche behaviors when non-Bean flux profiles are present? Are they diminished when the sensors cover only a small area of the sample?

The very nature of the "avalanching objects" is sometimes in question due to the lack of appropriate instruments for observation: are they individual vortices, or flux bundles? Are they rigid entities? Or perhaps we are seeing the irregular growth of tiny flux fingers, only visible with the most sophisticated instruments?

Imaging techniques suggest that some scenarios in which avalanches take place are quite different from the basic critical state of Bean. Catastrophic avalanches seem to be associated with "bursting," nonrepeatable dendritic structures, while noncatastrophic ones are mostly found in materials where the field penetrates as fingers with a Bean's-profile-like cross section. Even "roughness" in the critical state can be related to vortex avalanches, but this relation is only beginning to be properly established. Magneto-optical imaging seems to have the potential to realize our most extravagant dreams in vortex avalanche studies: high spatial and temporal resolution and the ability to take "magnetic pictures" of an ample region of the sample. This technique is limited only by the speed of data acquisition and data storage capabilities . . . but, with a little patience, these will find their way from Hollywood special effects departments to scientific laboratories.

All in all, it is clear that there are more questions than answers in the field of vortex avalanches. This is of course good news for the scientists working in complex systems, but probably even better news for the vortex physics community, which is occupied these days refining on the equilibrium H-T diagram of superconductors.

ACKNOWLEDGMENTS

The authors acknowledge useful discussions with Ch. Aegerter, P. Bak, K. E. Bassler, A. J. Batista-Leyva, K. Behnia, E. H. Brandt, J. R. Clem, T. Giamarchi, A. Gurevich, H. Herrmann, H. Jaeger, H. J. Jensen, P. Leiderer, X. S. Ling, J. Luzuriaga, M. C. Marchetti, M. Marchevsky, R. Mulet, E. Nowak, M. Paczuski, G. Parisi, H. Pastoriza, O. Ramos, G. Reiter, B. U. Runge, G. Seidler, D. V. Shantsev, O. Sotolongo, V. Vinokur, R. J. Wijngaarden, Y. Yeshurun, and E. Zeldov. We thank Å. F. Olsen for magneto-optical imaging work carried out specifically for this paper. E.A. thanks A. Rivera, J. Altshuler, and M. Álvarez for inspiration and support, and also the ACLS/SSRC Working Group on Cuba for online access to bibliographic materials. T.H.J. is grateful for financial support from the Norwegian Research Council.

REFERENCES

Abrikosov, A. A., 1957, Sov. Phys. JETP **5**, 1174.
Aegerter, C. M., 1998, Phys. Rev. E **58**, 1438.
Aegerter, C. M., M. S. Welling, and R. J. Wijngaarden, 2003, cond-mat/0305591.
Altshuler, E., 2001, in *Some Contemporary Problems in Condensed Matter Physics*, edited by S. J. Vlaev, L. M. Gaggero-Sager, and V. Droeglazov, Contemporary Fundamental Physics (Nova Science, Commack, NY), p. 65.
Altshuler, E., T. H. Johansen, Y. Paltiel, P. Jin, O. Ramos, K. E. Bassler, G. Reiter, E. Zeldov, and C. W. Chu, 2002, cond-mat/0208266.
Altshuler, E., O. Ramos, C. Martínez, L. E. Flores, and C. Noda, 1999, Phys. Rev. Lett. **86**, 5490.
Aranson, I., A. Gurevich, and V. Vinokur, 2001, Phys. Rev. Lett. **87**, 067003.
Avnir, D., O. Biham, D. Lidar, and O. Malcai, 1998, Science **279**, 39.
Bak, P., 1996, *How Nature Works—The Science of Self-Organized Criticality* (Copernicus, New York).
Bak, P., C. Tang, and K. Wiesenfeld, 1987, Phys. Rev. Lett. **77**, 111.
Barford, W., 1997, Phys. Rev. B **56**, 425.
Barford, W., W. H. Bee, and M. Steer, 1993, J. Phys.: Condens. Matter **5**, L333.
Barone, A., and G. Paternó, 1982, *Physics and the Applications of the Josephson Effect* (Academic, New York).
Bassler, K. E., and M. Paczuski, 1998, Phys. Rev. Lett. **81**, 3761.
Bassler, K. E., M. Paczuski, and E. Altshuler, 2001, Phys. Rev. B **64**, 224517.

Bassler, K. E., M. Paczuski, and G. Reiter, 1999, Phys. Rev. Lett. **83**, 3956.
Bean, C. P., 1962, Phys. Rev. Lett. **8**, 250.
Behnia, K., C. Capan, D. Mailly, and B. Etienne, 2000, Phys. Rev. B **61**, 3815.
Bending, S. J., 1999, Adv. Phys. **48**, 449.
Blatter, G., M. V. Feigel'man, V. B. Geshkenbein, A. I. Larkin, and V. M. Vinokur, 1994, Rev. Mod. Phys. **66**, 1125.
Blatter, G., V. B. Geshkenbein, and V. M. Vinokur, 1991, Phys. Rev. Lett. **66**, 3297.
Bobyl, A. V., D. V. Shantsev, Y. M. Galperin, Å. F. Olsen, T. H. Johansen, W. N. Kang, and S. I. Lee, 2003, cond-mat/0304603.
Bolz, U., 2002, *Magnetooptische Untersuchungen der Flussdynamik in YBaCuO-Filmen auf ultra-kurzen Zeitskalen*, Ph.D. thesis (University of Konstanz, Germany).
Bonabeau, E., and P. Lederer, 1995, Phys. Rev. B **52**, 494.
Bonabeau, E., and P. Lederer, 1996, Physica C **256**, 365.
Brandt, E. H., 1997, Phys. Rev. B **55**, 14 513.
Bretz, M., J. B. Cunningham, P. L. Kurczynski, and F. Nori, 1992, Phys. Rev. Lett. **69**, 2431.
Campbell, A. M., and J. E. Evetts, 1972, Adv. Phys. **21**, 199.
Carlson, J. M., and J. Doyle, 1999, Phys. Rev. E **60**, 1412.
Chen, Ch., and M. den. Nijs, 2002, Phys. Rev. E **66**, 011306.
Cruz, R., R. Mulet, and E. Altshuler, 2000, Physica A **275**, 15.
D'Anna, G., and F. Nori, 2000, Phys. Rev. Lett. **85**, 4096.
de Gennes, P. G., 1966, *Superconductivity of Metals and Alloys* (Benjamin, New York).
DeSorbo, W., and V. L. Newhouse, 1962, J. Appl. Phys. **33**, 1004.
Dingle, R., H. L. Störmer, A. C. Gossard, and W. Wiegman, 1978, Appl. Phys. Lett. **33**, 665.
Durán, C., P. L. Gammel, R. E. Miller, and D. J. Bishop, 1995, Phys. Rev. B **52**, 75.
Esquinazi, P., A. Setzer, D. Fuchs, Y. Kopelevich, and C. Assman, 1999, Phys. Rev. B **60**, 12 454.
Field, S., N. Venturi, and F. Nori, 1996, Phys. Rev. Lett. **74**, 74.
Field, S., J. Witt, F. Nori, and W. S. Ling, 1995, Phys. Rev. Lett. **74**, 1206.
Frette, V., K. Christensen, V. Malthe-Sørensen, J. Feder, T. Jøssang, and P. Meakin, 1996, Nature (London) **379**, 49.
Goa, P. E., H. Hauglin, M. Baziljevich, E. Il'yashenko, P. L. Gammel, and T. H. Johansen, 2001, Supercond. Sci. Technol. **14**, 729.
Heiden, C., and G. I. Rochlin, 1968, Phys. Rev. Lett. **21**, 691.
Held, G. A., D. H. Solina, D. T. Keane, W. J. Haag, P. M. Horn, and G. Grinstein, 1990, Phys. Rev. Lett. **65**, 1120.
Hope, A. P., M. J. Naughton, D. A. Gajewski, and M. B. Maple, 1999, Physica C **320**, 147.
Huang, Y., G. Ouillon, H. Saleur, and D. Sornette, 1997, Phys. Rev. E **55**, 6433.
Jaeger, H., 2000, private communication.
James, S. S., S. B. Field, J. Siegel, and H. Shtrikman, 2000, Physica C **332**, 445.
Jensen, H. J., 1998, *Self Organized Criticality—Emergent Complex Behaviour in Physical and Biological Systems* (Cambridge University, Cambridge, UK).
Johansen, T. H., M. Baziljevich, D. V. Shantsev, P. E. Goa, Y. M. Galperin, W. N. Kang, H. J. Kim, E. M. Choi, M.-S. Kim, and S. I. Lee, 2001, Supercond. Sci. Technol. **14**, 726.
Johansen, T. H., M. Baziljevich, D. V. Shantsev, P. E. Goa, Y. M. Galperin, W. N. Kang, H. J. Kim, E. M. Choi, M.-S. Kim, and S. I. Lee, 2002, Europhys. Lett. **59**, 599.
Kadanoff, L. P., S. R. Nagel, L. Wu, and S. Zhou, 1989, Phys. Rev. A **39**, 6524.
Kardar, M., G. Parisi, and Y. C. Zhang, 1986, Phys. Rev. Lett. **56**, 889.
Kelvin, Lord, 1884, see W. Thomson.
Kim, Y. B., C. F. Hempstead, and A. Strnad, 1963, Phys. Rev. **131**, 2486.
Koblischka, M. R., and R. W. Wijngaarden, 1995, Supercond. Sci. Technol. **8**, 199.
Kopelevich, Y., and S. Moehlecke, 1998, Phys. Rev. B **58**, 2834.
Larkin, A. I., and Yu. N. Ovchinnikov, 1973, Zh. Eksp. Teor. Fiz. **65**, 1704 [JETP **38**, 854].
Larkin, A. I., and Yu. N. Ovchinnikov, 1979, J. Low Temp. Phys. **34**, 409.
Lee, T. S., N. Missert, L. T. Sagdahl, J. Clarke, J. R. Clem, K. Char, J. N. Ekstein, D. K. Fork, L. Lombardo, L. A. Kapitulnik, L. F. Schneemeyer, J. V. Waszczak, and R. B. Van Dover, 1993, Phys. Rev. Lett. **74**, 2796.
Leiderer, P., J. Boneberg, P. Brüll, V. Bujok, and S. Herminghaus, 1993, Phys. Rev. Lett. **71**, 2646.
Milner, A., 2001, Physica C **294-295**, 388.
Mints, R. G., and A. L. Rakhmanov, 1981, Rev. Mod. Phys. **53**, 551.
Mulet, R., R. Cruz, and E. Altshuler, 2001, Phys. Rev. B **63**, 094501.
Newman, M. E. J., and K. Sneppen, 1996, Phys. Rev. E **54**, 6226.
Nowak, E. R., O. W. Taylor, L. Liu, H. M. Jaeger, and T. J. Selinder, 1997, Phys. Rev. B **55**, 11 702.
O'Brien, K. P., and M. B. Weissman, 1992, Phys. Rev. A **46**, R4475.
Olson, C. J., C. Reichhardt, J. Groth, S. B. Field, and F. Nori, 1997, Physica C **290**, 89.
Olson, C. J., C. Reichhardt, and F. Nori, 1997, Phys. Rev. B **56**, 6175.
Ooi, S., T. Shibaushi, and T. Tamegai, 2000, Physica C **284-288**, 775.
Oral, A., S. J. Bending, and M. Henini, 1996, Appl. Phys. Lett. **69**, 1324.
Paczuski, M., and K. E. Bassler, 2000, Phys. Rev. E **62**, 5347.
Pan, W., and S. Doniach, 1994, Phys. Rev. B **49**, 1192.
Pearl, J., 1964, Appl. Phys. Lett. **5**, 65.
Plá, O., N. K. Wilkin, and H. J. Jensen, 1996, Europhys. Lett. **33**, 297.
Plourde, B., F. Nori, and M. Bretz, 1993, Phys. Rev. Lett. **71**, 2749.
Prozorov, R., and D. Giller, 1999, Phys. Rev. B **59**, 14 687.
Radovan, H. A., and R. J. Zieve, 2003, Phys. Rev. B **68**, 224509.
Richardson, R. A., O. Plá, and F. Nori, 1994, Phys. Rev. Lett. **72**, 1268.
Rosendahl, J., M. Vekic, and J. Kelley, 1993, Phys. Rev. E **47**, 1401.
Rosendahl, J., M. Vekic, and J. Rutledge, 1994, Phys. Rev. Lett. **73**, 537.
Rudnev, I. A., S. V. Antonenko, D. V. Shantsev, T. H. Johansen, and A. E. Primenko, 2003, Cryogenics **43**, 663.
Runge, B. U., U. Bolz, J. Eisenmenger, and P. Leiderer, 2000, Physica C **341-348**, 2029.
Schwarz, J. M., and D. S. Fisher, 2001, Phys. Rev. Lett. **87**, 096107.
Seidler, G. T., C. S. Carrillo, T. F. Rosenbaum, U. Welp, G. W. Crabtree, and V. M. Vinokur, 1993, Phys. Rev. Lett. **70**, 2814.

Shung, E., T. F. Rosenbaum, and M. Sigrist, 1998, Phys. Rev. Lett. **80**, 1078.
Stoddart, S. T., S. J. Bending, A. K. Geim, and M. Henini, 1993, Phys. Rev. Lett. **71**, 3854.
Stoddart, S. T., S. J. Bending, A. K. Geim, and M. Henini, 1995, Supercond. Sci. Technol. **8**, 459.
Surdeanu, R., R. J. Wijngaarden, E. Visser, J. M. Huijbregtse, J. H. Rector, B. Dam, and R. Griessen, 1999, Phys. Rev. Lett. **83**, 2054.
Tang, C., 1993, Physica A **194**, 315.
Thomson, W. (Lord Kelvin), 1884, in *Lectures on Molecular Dynamics and the Wave Theory of Light* (Johns Hopkins University, Baltimore).
Vinokur, V., 2001, private communication.
Vinokur, V. M., M. V. Feigel'man, and V. B. Geshkenbein, 1991, Phys. Rev. Lett. **67**, 915.
Wang, Z., and D. Shi, 1993, Phys. Rev. B **48**, 9782.
Wertheimer, M. R., and J. le G. Gilchrist, 1967, J. Phys. Chem. Solids **28**, 2509.
Wischmeyer, C. R., 1967, Phys. Rev. **154**, 323.
Yeshurun, Y., A. P. Malozemoff, and A. Shaulov, 1996, Rev. Mod. Phys. **68**, 911.
Zeldov, E., J. R. Clem, M. McElfresh, and M. Darwin, 1994, Phys. Rev. B **49**, 9802.
Zieve, R. J., T. F. Rosenbaum, H. Jaeger, G. T. Seidler, G. W. Crabtree, and U. Welp, 1996, Phys. Rev. B **53**, 11 849.